Direct Georeferecing of Fire Front Aerial Images using Iterative Ray-Tracing and a Bearings-Range Extended Kalman Filter

Bernardo Santana[2]
bernardo.santana@tecnico.ulisboa.pt
Alexandre Bernardino[1]
alex@isr.tecnico.ulisboa.pt
Ricardo Ribeiro[1]
ribeiro@isr.tecnico.ulisboa.pt

[1] Institute for Systems and Robotics
Instituto Superior Técnico
Lisbon, Portugal

[2] MSc Student,
Instituto Superior Técnico
Lisbon, Portugal

Abstract

This paper discusses the design and implementation of the Iterative Ray-Tracing algorithm for forest fire georeferencing using aerial imagery, a Global Positioning System (GPS), an Inertial Measurement Unit (IMU) and a Digital Elevation Model (DEM). Taking into account that measurement errors are amplified by the target distance, an Extended Kalman Filter (EKF) is proposed to filter multiple observations of the same object of interest. This filter extracts the bearings and range information from the geometric relation between the target and the camera in a local coordinate system. A performance comparison is done with a Cubature Kalman Filter (CKF) considering possible linearization errors induced by the EKF.

In order to validate the georeferencing and filtering algorithms, an experiment was conducted. A mobile phone was used to acquire GPS, IMU and 14 images of a target. An average position error of 74.483m was obtained at an average distance of 605m. Applying the Bearings-Range EKF and CKF reduced the error to 33.620 and 33.820, respectively.

1 Introduction

Forest fires are increasingly becoming a frequent problem in modern day society. Their destructive potential makes them a serious concern and a challenge for firefighting authorities.

Fire propagation models have already been studied that take into account weather variables such as wind [7] and also the terrain type [6]. However, these models usefulness is limited since no fire geolocation algorithm has been developed for this purpose. Henceforth, the aim of this work is to fill in this gap and develop a georeferencing algorithm based on images and telemetry recorded by an aerial vehicle. This images are assumed to be pre-processed to identify the pixels that correspond to fire.

1.1 Related Work

Forlani et al. [3] apply direct georeferencing by using the on-board Global Navigation Satellite System with the Real-Time Kinematic option with Structure from Motion and Bundle Adjustment. No ground control points are used. This methodology is, however, not suitable in a forest fire scenario, where the lack of differentiated texture and smoke prevents feature extraction and matching.

Conte et al. [2] propose an image registration approach by pattern-matching the images collected from a Micro Aerial Vehicle with satellite imagery. Multiple measurements are taken and recursive least square filter is applied. Similarly to [3], this technique relies on feature extraction, and is therefore unreliable in a forest fire environment.

Ponda et al. [8] develop a Line-of-Sight Bearings-Only EKF for target localization. This requires, however, a prior knowledge of the target's position, which is not reviewed in that work. Xu et al. [10] propose the same measurement model using a CKF instead, considering possible linearization errors induced by the standard EKF. To determine an initial approximation of the target's position, the Iterative Photogrammetry (IP) algorithm [9] is used. In spite of being efficient, the IP method can diverge when the incidence angle is smaller than the profile inclination angle.

Leira et al. [5] propose the intersection of the optic ray with a flat surface. This generalization, however, is not suitable in rough terrains, as seen in [10].

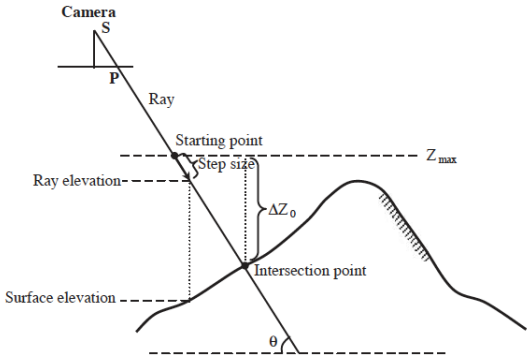

Figure 1: Iterative Ray-Tracing (adapted from [9]).

2 Georeferencing Algorithm - Iterative Ray-Tracing

The proposed georeferencing algorithm is the Iterative Ray-Tracing (IRT) [9], presented in Figure 1, and the DEM used is the EU-DEM v1.1 [1], with a spatial resolution of 25 meters and georeferenced in EPSG:3035. Since the purpose of this work is to output the geodetic coordinates of the target, this map is converted to the EPSG:4326.

The IRT works by extending the optic ray with a step size until it hits the surface. A GPS and IMU are needed to define the origin and direction of this ray, respectively, in a local NED frame. The intersection is detected when the point elevation is equal or smaller than the elevation of the DEM.

Multiple upgrades were introduced in the basic IRT, including a dynamic step size, to increase the accuracy of the algorithm. Furthermore, the starting iteration point was set as the intersection of the ray with the maximum elevation of the loaded DEM. It is expected that the aerial vehicles will operate at heights greater than the local terrain, and this can reduce the number of iterations considerably. Finally, bilinear interpolation was implemented to refine the elevation of the queried point. Ghandehari et al. [4] concluded in their work that for DEM's with finer resolutions, such has the EU-DEM v1.1, this type of interpolation achieves good results with low processing times.

3 Bearings-Range Filter

3.1 Target Dynamic Model

In this work, the target is assumed to be stationary. Therefore, its dynamics can be modeled by $\mathbf{t}_{k+1} = \Phi_{k+1|k}\mathbf{t}_k + \mathbf{Q}_k$, where $\mathbf{t}_k$ represents the target position, $\Phi_{k+1|k}$ the state transition matrix and $\mathbf{Q}_k$ the process covariance matrix:

$$\Phi_{k+1|k} = \begin{bmatrix} 1 & 0 & 0 \\ 0 & 1 & 0 \\ 0 & 0 & 1 \end{bmatrix}, \quad \mathbf{Q}_k = \begin{bmatrix} 0 & 0 & 0 \\ 0 & 0 & 0 \\ 0 & 0 & 0 \end{bmatrix}. \tag{1}$$

3.2 Bearings-Range Measurement Model

The measurement model is given by $\mathbf{z}_{k+1} = \mathbf{h}(\mathbf{t}_{k+1}) + \mathbf{R}_k$, where $\mathbf{z}_{k+1}$ is the new measurement, $\mathbf{h}$ is the non-linear measurement function and $\mathbf{R}_k$ is the measurement noise covariance matrix.

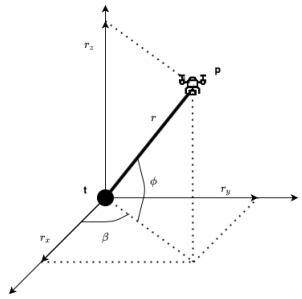

Figure 2: Bearings-Range model geometry.

$$\mathbf{h}(\mathbf{t}_{k+1}) = \begin{bmatrix} \beta \\ \phi \\ r \end{bmatrix} = \begin{bmatrix} \tan^{-1}\left(\frac{p_y - t_y}{p_x - t_x}\right) \\ \tan^{-1}\left(\frac{p_z - t_z}{\sqrt{(p_x-t_x)^2+(p_y-t_y)^2}}\right) \\ \sqrt{(p_x-t_x)^2+(p_y-t_y)^2+(p_z-t_z)^2} \end{bmatrix}, \quad (2)$$

where β and ϕ are the azimuth and elevation angles, respectively, and r is the distance between the target, $\mathbf{t}$, and the aerial vehicle, $\mathbf{p}$, as presented in Figure 2.

4 Experiment

The unavailability of telemetry and imagery data from an aerial vehicle led to the development of an alternative methodology to validate the proposed algorithm. A mobile phone was used to record GPS, IMU and image data along a pedestrian path. The natural elevation of *Serra dos Candeeiros*, near *Porto de Mós*, *Leiria*, was used to capture images of a target at a lower height, so as to simulate the overview of an aerial vehicle. A total of 14 images were acquired at an average target distance of 605 meters. For the filtering, the IRT result for the first observation is used to initialize the filter state, $\mathbf{t}_0$. The initial state covariance $\mathbf{P}_0$ and measurement noise covariance matrix $\mathbf{R}_k$ were tuned to

$$\mathbf{P}_0 = \begin{bmatrix} 20^2 & 0 & 0 \\ 0 & 50^2 & 0 \\ 0 & 0 & 1^2 \end{bmatrix}, \quad \mathbf{R}_k = \begin{bmatrix} 5^2 & 0 & 0 \\ 0 & 5^2 & 0 \\ 0 & 0 & 10^2 \end{bmatrix}. \quad (3)$$

Details on the EKF and CKF algorithms can be found in [8] and [10], respectively.

The position error is defined as $\mathbf{e_p} = \mathbf{t} - \hat{\mathbf{t}}$, where $\hat{\mathbf{t}}$ is the estimated target. σ_x, σ_y and σ_z are defined as the square root of the filter state covariance matrix diagonal. The results of the standalone IRT, EKF and CKF are summarized in Table 1.

Method	$\|\|e_p\|\|$ [m]	$\|\|\sigma_{x,y,z}\|\|$ [m]
IRT	74.483	n.d.
IRT+EKF	33.620	7.2497
IRT+CKF	33.820	7.2502

Table 1: Norm of the average position error for the standalone IRT and for the final correction of the EKF and CKF.

The IRT results presented in Figure 3 evidence a bias along the positive East direction, which then influences the estimated positions of the EKF and CKF.

5 Conclusions

In this paper, the IRT is proposed as a georeferencing algorithm using the EU-DEM v1.1. Expecting measurement errors from the GPS and IMU, a bearings-range filtering algorithm was developed, with a performance comparison between the EKF and CKF. Preliminary results using the data collected with a mobile phone show evidence of bias susceptibility. This may be due to the non-ideal preliminary experimental setup using a line of sight more parallel to the ground when compared to the more vertical one from an aerial vehicle. Furthermore, the 14 images were captured at approximate positions, limiting the new information added to the filtering algorithm. Still, an improvement of 41 meters is achieved on the 74 meter

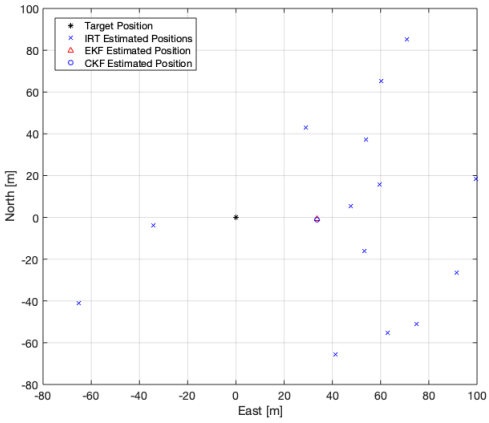

Figure 3: Real and estimated target positions by the IRT, EKF and CKF algorithms.

average position error of the standalone IRT. There is no clear advantage in using the CKF over the EKF for this measurement model.

Acknowledgements

This work was supported by FCT with the LARSyS - FCT Project UIDB/50009/2020 and project FIREFRONT (PCIF/SSI/0096/2017).

References

[1] EU-DEM v1.1. URL `https://land.copernicus.eu/imagery-in-situ/eu-dem/eu-dem-v1.1`. visited on 26-07-2020.

[2] Gianpaolo Conte, Maria Hempel, Piotr Rudol, David Lundström, Simone Duranti, Mariusz Wzorek, and Patrick Doherty. High accuracy ground target geo-location using autonomous micro aerial vehicle platforms. *AIAA Guidance, Navigation and Control Conference and Exhibit*, pages 1–14, 2008.

[3] Gianfranco Forlani, Fabrizio Diotri, Umberto Morra di Cella, and Riccardo Roncella. Indirect UAV Strip Georeferencing by On-Board GNSS Data under Poor Satellite Coverage. *Remote Sensing*, 11(15):1765, 2019.

[4] Mehran Ghandehari, Barbara P Buttenfield, and Carson J Q Farmer. Comparing the accuracy of estimated terrain elevations across spatial resolution. *International Journal of Remote Sensing*, 40(13): 5025–5049, 7 2019.

[5] Frederik S. Leira, Kenan Trnka, Thor I. Fossen, and Tor Arne Johansen. A ligth-weight thermal camera payload with georeferencing capabilities for small fixed-wing UAVs. *2015 International Conference on Unmanned Aircraft Systems, ICUAS 2015*, pages 485–494, 2015.

[6] A. M.G. Lopes, A. C.M. Sousa, and D. X. Viegas. Numerical simulation of turbulent flow and fire propagation in complex topography. *Numerical Heat Transfer; Part A: Applications*, 27(2):229–253, 2 1995.

[7] A. M.G. Lopes, L. M. Ribeiro, D. X. Viegas, and J. R. Raposo. Simulation of forest fire spread using a two-way coupling algorithm and its application to a real wildfire. *Journal of Wind Engineering and Industrial Aerodynamics*, 193(July):103967, 2019.

[8] Sameera S. Ponda, Richard M. Kolacinski, and Emilio Frazzoli. Trajectory optimization for target localization using small unmanned aerial vehicles. *AIAA Guidance, Navigation, and Control Conference and Exhibit*, (August), 2009.

[9] Yongwei Sheng. Comparative evaluation of iterative and non-iterative methods to ground coordinate determination from single aerial images. *Computers and Geosciences*, 30(3):267–279, 2004.

[10] Cheng Xu, Daqing Huang, and Jianye Liu. Target location of unmanned aerial vehicles based on the electro-optical stabilization and tracking platform. *Measurement*, 147, 12 2019.

*/